JOURNAL OF APPLIED ELECTROCHEMISTRY 21 (1991) 785–792

# Correlation between mass transfer and operating parameters in zinc electrowinning

A. Y. HOSNY, T. J. O'KEEFE, J. W. JOHNSON, W. J. JAMES

*Departments of Chemical Engineering, Metallurgical Engineering, and Chemistry and Graduate Center for Materials Research, University of Missouri-Rolla, Rolla, Missouri 65401, USA*

Received 30 March 1990; revised 14 February 1991

The effects of antimony additions, acid concentration, and current density on mass transfer and deposition morphology were examined. The mass transfer coefficients of zinc were calculated using a codeposition method with cadmium as a tracer. The experiments were carried out for vertical electrodes in a Hull cell. The results indicate that the mass transfer coefficients increase with increasing antimony additions, acid concentration, and current density. Zinc dissolution is more severe at low current density and higher antimony levels than at higher current densities and lower antimony levels. A mass transfer correlation for pure zinc electrolyte data is

$$Sh = 12.47(ReSc)^{0.45}$$

where *Sh*, *Re*, and *Sc* are the Sherwood, Reynolds, and Schmidt numbers, respectively. The correlation fits very well with the experimental data. A correlation for electrolytes containing antimony was also obtained and has an exponent of 0.42. The correlations cover a wide range of operating parameters and provide a fast quantitative estimation of the change in mass transfer in zinc electrowinning.

## 1. Introduction

The study of mass transfer at gas-evolving electrodes is of great interest to electrochemical industries, such as zinc electrowinning, where hydrogen gas bubbles evolve simultaneously with zinc deposition. In general, mass transfer at gas-evolving electrodes, is strongly influenced by the volume flux of gas evolved at the electrode surface. A number of parameters influencing nucleate gas evolution have been investigated such as electrode position, temperature, nature of gas, pressure and surface roughness [1–4]. Impurities such as antimony decrease the zinc deposition current efficiency due to the increase in the volume flux of hydrogen gas which affects the mass transfer coefficient. Since hydrogen gas evolution and antimony concentration are related, research was conducted to investigate the effect of antimony on the zinc mass transfer coefficient. In general, impurity relations associated with mass transfer are not among the subjects which are familiar to the field of electrochemistry. Consequently, little attention has been focused on the problem of low concentration impurity relationships. Thus, a major objective of this study was to determine the influence of antimony and sulphuric acid concentration on the zinc mass transfer coefficients.

Investigators of mass transfer enhancement at gas-evolving electrodes have generally reported their correlations as follows:

$$K_d = \text{const}\ (V_g/A)^m \quad (1)$$

where $K_d$ = mean mass transfer coefficient (cm s$^{-1}$), $V_g$ = volume flow rate (cm$^3$ min$^{-1}$), $A$ = area of electrode (cm$^2$), $V = V_g/A$ = volume flux (cm$^3$ cm$^{-2}$ min$^{-1}$) and $m$ = a numerical value varying from 0.25 to 0.87 [5]. The mass transfer coefficient is related to the diffusion layer thickness by the equation

$$\delta = D/K_d \quad (2)$$

where $\delta$ = diffusion layer thickness (cm) and $D$ = diffusion coefficient (cm$^2$ s$^{-1}$).

Other investigators [6] utilize the equation:

$$\delta = \text{const}\ (V_g/A)^{-m} \quad (3)$$

Several models have been proposed for describing the mechanism of mass transfer enhancement through gas evolution [7–10]. In the penetration model, Ibl and Venczel [7] have suggested that the detachment of bubbles from the electrode creates an empty space, which is filled by solution from the bulk. The electroactive species then diffuse toward the electrode until the next bubble starts growing at the same nucleation site. During this period between the growth of bubbles, the theory assumes that mass transfer is governed predominantly by non-steady diffusion in a quiescent liquid. The model can be presented in a simple form by the following equation:

$$Sh = \text{const}\ (ReSc)^{0.5}(1 - \theta)^{0.5} \quad (4)$$

where $Sh$ = Sherwood number = $KL/D$; $Re$ = Reynolds number = $Lv/\nu$; $Sc$ = Schmidt number = $\nu D^*$ $L$ = characteristic length of the electrode (cm); $v$ = discharge gas velocity (cm s$^{-1}$); $\nu$ = solution

0021-891X/91 $03.00 + .12 

viscosity ($cm^2\ s^{-1}$); and $\theta$ = fractional surface coverage that must be experimentally determined.

A variation of the Ibl model was presented by Rousar and Gezner [8]. The microconvection model proposed by Stephan and Vogt [9] considers that the growing bubble induces a liquid flow past the electrode surface. The velocity of the liquid flow is considered a decisive factor for mass transfer. The model differs from the penetration model mainly in that it assumes diffusion in a quiescent liquid to be absent and that only convective mass transfer is active. The model can be approximated for practical use by the following equation:

$$Sh = \text{const}\ (Re^{0.5} Sc^{0.487}) \quad (5)$$

The numerical results of the penetration and microconvection models do not differ essentially, except for an extremely small fraction of surface coverage.

Finally, in the hydrodynamic model proposed by Janssen and Barendrecht [10], the electrolyte flow caused by the lift effect of ascending bubbles is considered to be the governing factor in the mass transfer. The model appears to be applicable in cases where coalescence of the adhering bubbles does not occur [1]. The final presentation of the model can be given by:

$$Sh = \text{const}\ (ReSc)^{0.33} \quad (6)$$

Strock and others [11] have reported experimental mass transfer data which describe the connecting mechanism between mass and momentum transfer.

Since mass transfer coefficients can be determined using electrochemical tracer techniques [12–14], a series of experiments was conducted using the codeposition method with $Cd^{2+}$ as a tracer. The limiting current densities of $Cd^{2+}$ tracers were determined by chemical analysis, and the volume flux of the hydrogen gas was calculated using Faraday's law. In this work, the zinc ion mass transfer coefficients were determined at different current densities and the zinc deposit morphologies were examined by means of SEM. Attempts were made to characterize the effects of antimony and acid concentrations on the mass transfer coefficients in order to obtain a useful empirical correlation for practical applications. The correlations obtained have been compared with existing models to see if the results of our experiments are in agreement with any one model.

## 2. Experimental details

A Hull cell, 267 ml volume, which allows assessment of the deposits at varying current densities on a single test electrode, was used in this study and is described in the literature [15]. Aluminium working electrodes were prepared by a technique also described in the literature [16]. A single lead anode was used.

A power supply was used to drive the circuit. A total current of 2 A was applied for 20 min, to give a current distribution range from 2 to 80 mA $cm^{-2}$ at the electrode surface. The electrode edges were covered by electroplaters' tape so as to allow for homogeneous deposition. The electrode design allows separation into several sections, each with a separate range of current density [15]. For practical reasons, the current density range refers to the higher value allowed, e.g., for a section between 8 and 12 mA $cm^{-2}$, the current density is said to be 12 mA $cm^{-2}$. Experiments were also made using the codeposition method developed by Ettel *et al.* [12], using $Cd^{2+}$ as a tracer ion at a fixed level of 50 mg $dm^{-3}$ in the zinc electrolyte. The tests were carried out at ambient temperature, ~25° C.

Reagent grade chemicals were used in all experiments. The electrolyte was prepared by adding sulphuric acid to a slurry mixture of French Process zinc oxide powder and deionized water. Stock solutions of $Sb^{3+}$ and $Cd^{2+}$ were prepared by dissolving antimony-potassium tartarate and cadmium sulphate in deionized water. Test solutions were prepared in a 1 $dm^3$ volumetric flask by mixing the proper amounts of neutral zinc sulphate solution, reagent grade sulphuric acid, $Sb^{3+}$, $Cd^{2+}$, and deionized water. The kinematic viscosities of the electrolytes were measured with a size 50 Cannon-Fenske viscometer.

The deposits used for chemical analysis were obtained at current densities of 12, 30, 40, 50 and 60 mA $cm^{-2}$. The corresponding areas of the deposits were measured precisely for calculations. The zinc deposits obtained were weighed for current efficiency calculations. Subsequently, the volumes of hydrogen were calculated from the current efficiencies. Deposits at current densities 20 and 80 mA $cm^{-2}$ were used for morphological studies by SEM. The deposits obtained were dissolved in 5 $cm^3$ of 5 M $HNO_3$ and analysed by atomic absorption (AA) spectroscopy. The limiting current density of Cd was calculated from the amount of Cd in the deposits, since the Cd deposition was under diffusion control.

## 3. Results and discussion

### 3.1. *Antimony additions study*

Figure 1 shows the effect of antimony concentration on the zinc ion mass transfer coefficients, $K^*_{Zn}$, at different current densities for an electrolyte containing 50 g $dm^{-3}$ Zn, 150 g $dm^{-3}$ sulphuric acid. The zinc mass transfer coefficients increased with increasing antimony concentration in the electrolyte, e.g., $K_{Zn}$ at a current density of 30 mA $cm^{-2}$ was $3.98 \times 10^{-4}$ and $5.15 \times 10^{-4}$ cm $s^{-1}$ at 0.0 and 0.06 mg $dm^{-3}$ $Sb^{3+}$, respectively. In addition, an increase in current density caused a significant increase in the $K_{Zn}$ values as shown in Fig. 1. For example, for an electrolyte containing 0.06 mg $dm^{-3}$ $Sb^{3+}$, the $K_{Zn}$ value at a current density of 12 mA $cm^{-2}$ was $4.53 \times 10^{-4}$ cm $s^{-1}$ and at 60 mA $cm^{-2}$ was $6.70 \times 10^{-4}$ cm $s^{-1}$. The increase in current density is associated with a notable decrease in the diffusion layer thickness, $\delta_{Zn}$ (see Fig. 2) for an electrolyte containing 50 g $dm^{-3}$ Zn and 150 g $dm^{-3}$

* Throughout this manuscript, $K_{Zn}$, $D_{Zn}$, $\delta_{Zn}$, etc., the subscript refers to the metal ion.

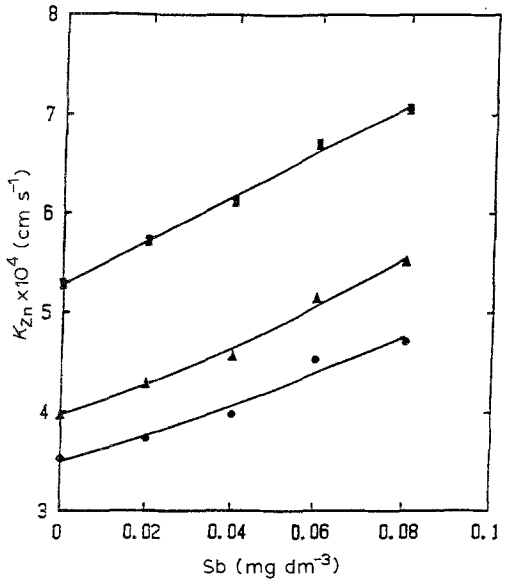


Fig. 1. The effect of antimony concentration and current density (c.d.) on $K_{Zn}$ for electrolyte containing 50 g dm$^{-3}$ Zn, 150 g dm$^{-3}$ $H_2SO_4$. c.d. (■) 60, (▲) 30 and (●) 12 mA cm$^{-2}$.

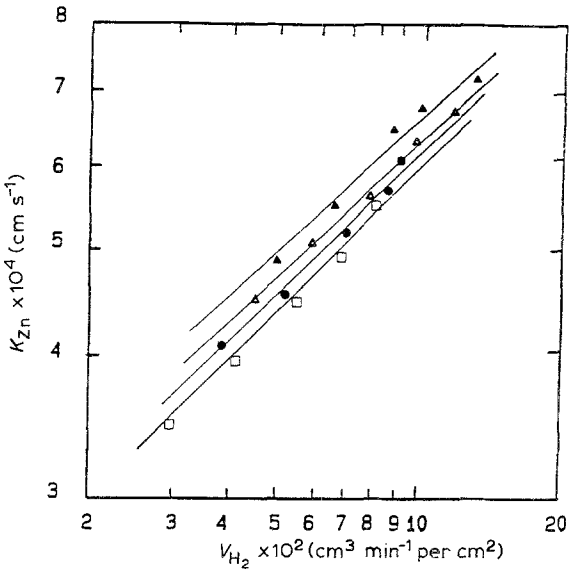


Fig. 3. Plot of $K_{Zn}$ values against volume flux of hydrogen for electrolyte containing 50 g dm$^{-3}$ $H_2SO_4$ and various concentrations of antimony: (□) 0.0, (●) 0.04, (△) 0.06 and (▲) 0.08 mg dm$^{-3}$.

$H_2SO_4$ with various $Sb^{3+}$ concentrations. In general, at all levels of antimony concentration, a constant decrease in $\delta_{Zn}$ was observed as the current density increased. Similar results were noted for electrolytes containing 50 g dm$^{-3}$ Zn with 100, 150 and 200 g dm$^{-3}$ sulphuric acid. The thickness of the diffusion layer represents the interaction of the dynamic forces due to electrolyte movement and viscous forces near the electrode surface. The presence of antimony in an electrolyte enhances the hydrogen evolution reaction, thus the volume flux increases, subsequent stirring of the solution occurs, and $\delta_{Zn}$ decreases. Since $\delta_{Zn}$ is related to $K_{Zn}$ via $D_{Zn}/K_{Zn}$ and $D_{Zn}$ is considered constant and equal to $3.8 \times 10^{-6}$ cm$^2$ s$^{-1}$ [16], an increase in the gas evolution enhances the mass transfer coefficients [17, 18]. The influence of the volume flux of hydrogen gas on $K_{Zn}$ is shown in Fig. 3 for a zinc electrolyte containing 50 g l$^{-1}$ $Zn^{2+}$, 150 g l$^{-1}$ $H_2SO_4$ over a current density range of 12–60 mA cm$^{-2}$. The gas volume flux was determined from experimental measurements of the current efficiencies and Faraday's law. Figure 3 shows that the increase in the $K_{Zn}$ values is associated with an increase in the hydrogen volume flux, e.g., $K_{Zn}$ values are $5.5 \times 10^{-4}$ and $7.1 \times 10^{-4}$ cm s$^{-1}$ for volume flux values of $8.17 \times 10^{-2}$ and $13.17 \times 10^{-2}$ cm$^3$ cm$^{-2}$ min$^{-1}$, respectively. Moreover, the slope, $m$, of lines in Fig. 3 for an antimony-free electrolyte is 0.44, in good agreement with values of 0.36 to 0.53 for hydrogen gas in acidic medium [5] reported in the literature. The $m = 0.44$ value is also close to the value of 0.47 obtained by Janssen and Hoogland [3] for a vertical electrode, similar to the electrode position in this study.

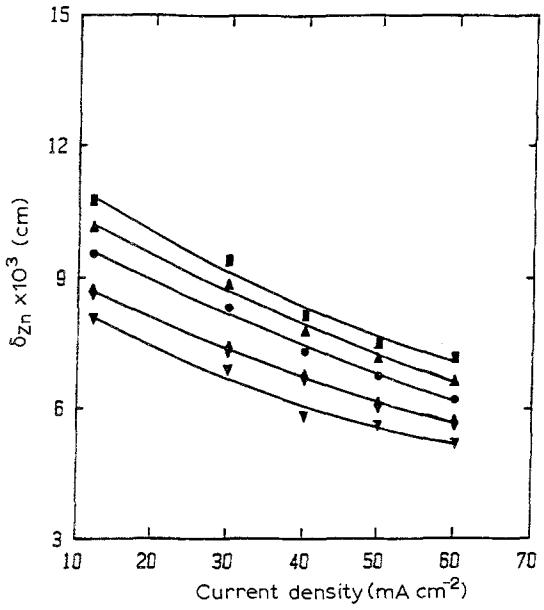


Fig. 2. Diffusion layer thickness of Zn obtained at different current densities for electrolytes containing 50 g dm$^{-3}$ Zn, 150 g dm$^{-3}$ $H_2SO_4$ and various antimony concentrations: (■) 0.0, (▲) 0.02, (●) 0.04, (◆) 0.06 and (▼) 0.08 mg dm$^{-3}$.

In general, the results shown in Figs 1, 2 and 3 focus attention on the enhancement of the mass transfer coefficients in the presence of antimony. The magnitude of the mass transfer coefficients changed significantly as antimony was added to the zinc electrolyte. At a fixed current density of 40 mA cm$^{-2}$, $K_{Zn}$ at 0.06 mg dm$^{-3}$ $Sb^{3+}$ increased by a factor of 1.21 relative to $K_{Zn}$ at 0.0 mg dm$^{-3}$ $Sb^{3+}$.

It was recognized that a rough deposit would be prevalent when the plating current density exceeded a certain fraction of the limiting current density, $I_l$. Thus, deposits obtained under conditions with higher limiting current densities should be smoother than those obtained at lower values. The mass transfer studies show that the presence of antimony in the electrolyte increases the limiting current densities of $Zn^{2+}$, see Tables 1 to 3. As discussed above, the mass transfer coefficients increase with the enhancement of volume flux, therefore, the roughening of deposits can be eliminated by increasing $K_{Zn}$. The SEM pictures for deposits obtained from an antimony-free electrolyte

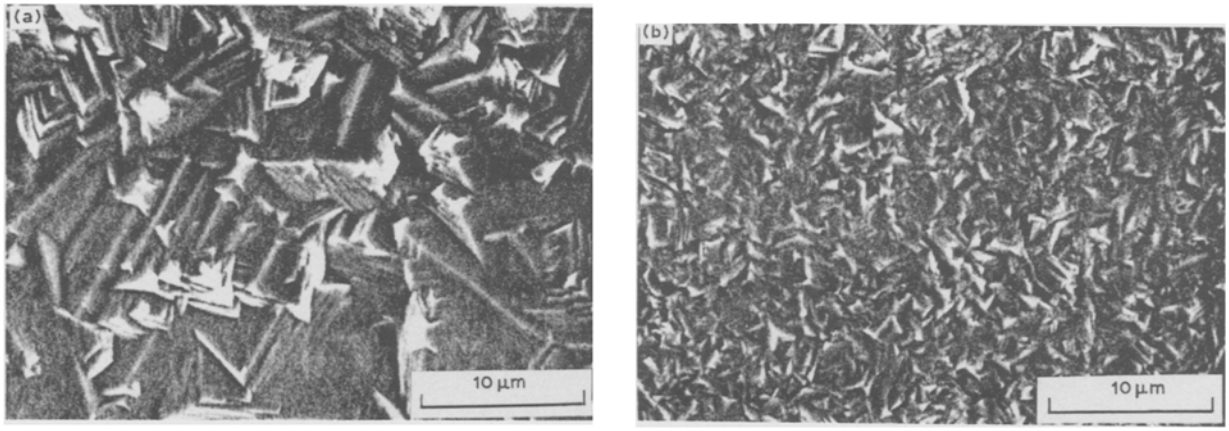


Fig. 4. Zn deposits obtained at 80 mA cm$^{-2}$ for an electrolyte containing 50 g dm$^{-3}$ Zn, 150 g dm$^{-3}$ $H_2SO_4$ with (a) 0.0 mg dm$^{-3}$ $Sb^{3+}$, (b) 0.04 mg dm$^{-3}$ $Sb^{3+}$ concentrations.

and with 0.04 mg dm$^{-3}$ antimony added are shown in Fig. 4a and b, respectively, at a current density of 80 mA cm$^{-2}$ for 50 g dm$^{-3}$ $Zn^{2+}$, 150 g dm$^{-3}$ $H_2SO_4$. Figure 4 shows that there is a tendency for Zn to develop a finer grain size in electrolytes with higher $K_{Zn}$ values. This result appears contrary to the behaviour reported by Winand [19]. However, the increased mass transfer in this case enhances the antimony effect which dominates the observed morphology. Thus, the increase in $K_{Zn}$ is a consequent of the antimony which in turn enhances the volume flux of hydrogen. Therefore, the finer faceting size exhibited by the micrographs is consistent with this explanation and is not in conflict with the observations of Winand.

The effect of antimony at a low current density value, 20 mA cm$^{-2}$, on the deposition morphology is shown in Figs 5a, 5b and 6a for an electrolyte containing 50 g dm$^{-3}$ $Zn^{2+}$, 150 g dm$^{-3}$ $H_2SO_4$ with antimony concentrations of 0.0, 0.04 and 0.08 mg dm$^{-3}$, respectively. The surface of the deposit deteriorates as the antimony concentrations increase, e.g., at 0.04 mg dm$^{-3}$ $Sb^{3+}$, the grain boundary edges are more rounded, Fig. 5b. A significant change in morphology is also seen, Fig. 6a, for deposits obtained from an electrolyte containing 0.08 mg dm$^{-3}$ $Sb^{3+}$ against an antimony-free electrolyte. In addition to the structure seen in Fig. 5b, there is a noticeable dissolution of zinc as indicated by separated grains and rounded edges. The deformation of the deposit may be due to the enhancement of hydrogen evolution resulting from the presence of a higher antimony concentration or antimony absorption on the electrode surface. A comparison of the deposit morphologies at 80 and 20 mA cm$^{-2}$ is shown by SEM pictures in Fig. 6a and b. At higher current densities, the deposit is more compact and visibly less attacked.

The increase in current density enhances both forced and free convection. Forced convection is due to the increase in the volume flux of gas; natural convection is due to the density difference, accompanying the concentration gradient, between the electrode surface and the bulk of the solution. The mass transfer studies indicate that $K_{Zn}$ increases by a factor of 1.4 when the current density is increased from 12 to 60 mA cm$^{-2}$ for a 50 g dm$^{-3}$ Zn, 150 g dm$^{-3}$ $H_2SO_4$ electrolyte containing either none or 0.08 mg dm$^{-3}$ $Sb^{3+}$. For the same conditions, the change in the magnitude of the volume flux of hydrogen gas is 2.63. Again, the micrographs in Figs 5 and 6 show that the effect of the antimony additions is to dominate the surface structure, particularly at low current densities.

### 3.2. *Acid study*

Figure 7 gives the variation in $K_{Zn}$ with $H_2SO_4$ concentration at current densities of 30 and 60 mA cm$^{-2}$ for an electrolyte containing 50 g dm$^{-3}$ $Zn^{2+}$ with 0.00 mg dm$^{-3}$ and 0.02 mg dm$^{-3}$ $Sb^{3+}$. The $K_{Zn}$ values increase with increasing sulphuric acid concentrations, e.g., for an antimony-free electrolyte and at 30 mA cm$^{-2}$, the $K_{Zn}$ values are $3.6 \times 10^{-4}$ and $4.45 \times 10^{-4}$ cm s$^{-1}$ for 100 and 200 g dm$^{-3}$ $H_2SO_4$,

*Table 1. Calculation of Sc, Sh, and Sc/Re numbers for different plating current densities in an electrolyte containing 50 g dm$^{-3}$ Zn and 100 g dm$^{-3}$ $H_2SO_4$*

| | | | | | |
|---|---|---|---|---|---|
| c.d. (mA cm$^{-2}$) | 60 | 50 | 40 | 30 | 12 |
| $K_{Zn} \times 10^4$ (cm s$^{-1}$) | 4.9 | 4.7 | 4.3 | 3.6 | 3.2 |
| $I_{l,Zn}$ (mA cm$^{-2}$) | 77.4 | 73.5 | 67.8 | 56.5 | 50.3 |
| $\rho$ (g cm$^{-3}$) | 1.076 | 1.087 | 1.093 | 1.103 | 1.136 |
| $\nu \times 10^2$ (cm$^2$ s$^{-1}$) | 1.286 | 1.304 | 1.326 | 1.342 | 1.449 |
| *Sc* | 3383 | 3432 | 3489 | 3532 | 3812 |
| *Sh* | 194 | 185 | 170 | 142 | 126 |
| $\delta_{Zn} \times 10^3$ (cm) | 7.71 | 8.11 | 8.81 | 10.56 | 11.87 |
| *Sc/Re* | 478 | 398 | 318 | 239 | 187 |
| *Sc/Gr* $\times 10^{-9}$ | 2.824 | 2.756 | 2.687 | 2.638 | 2.374 |

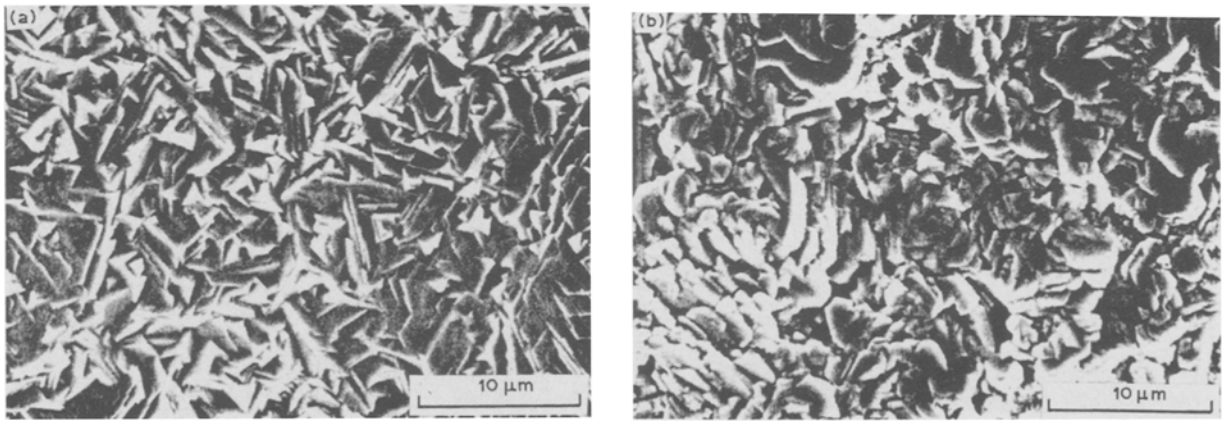


Fig. 5. Zn deposits obtained from an electrolyte containing 50 g dm$^{-3}$ Zn, 150 g dm$^{-3}$ $H_2SO_4$ at 20 mA cm$^{-2}$ with (a) 0.0 mg dm$^{-3}$ $Sb^{3+}$, (b) 0.04 mg dm$^{-3}$ $Sb^{3+}$ concentrations.

respectively. In addition, the plots in Fig. 7 indicate that the increase in the current density from 30 to 60 mA cm$^{-2}$ enhances the $K_{Zn}$ values at a fixed acid concentration. For example, the $K_{Zn}$ values are $3.6 \times 10^{-4}$ and $4.9 \times 10^{-4}$ cm s$^{-1}$ for 30 and 60 mA cm$^{-2}$, respectively, for a 50 g dm$^{-3}$ $Zn^{2+}$ electrolyte containing 100 g dm$^{-3}$ $H_2SO_4$. A similar trend was observed for electrolytes containing $Sb^{3+}$ as also shown in Fig. 7 for 0.02 mg dm$^{-3}$ $Sb^{3+}$. The acid concentration used in the experiment is similar to that used in zinc electrowinning. The results shown in Fig. 8 represent the change of $K_{Zn}$ at several levels of $Sb^{3+}$ concentration in electrolytes containing acid concentrations from 100 to 200 g dm$^{-3}$, for a fixed current density such as 60 mA cm$^{-2}$. For example, the values of $K_{Zn}$ for an electrolyte containing 50 g dm$^{-3}$ Zn and 0.06 mg dm$^{-3}$ $Sb^{3+}$ are $6.1 \times 10^{-4}$ and $6.9 \times 10^{-4}$ cm$^{-1}$ for 100 and 200 g dm$^{-3}$ acid, respectively.

The increase in the $K_{Zn}$ values at higher acid concentrations is due to the enhancement of hydrogen generation at the electrode surface. The relations between the volume flux of hydrogen gas evolved and $K_{Zn}$ at several acid concentrations are shown in Fig. 9. The acid concentrations varied from 100 to 200 g dm$^{-3}$ and the current densities varied from 12 to 60 mA cm$^{-2}$. The slopes of the lines obtained, $m$, are 0.47, 0.44, and 0.38 for 100, 150, and 200 g dm$^{-3}$ sulphuric acid, respectively, for antimony-free electrolytes containing 50 g dm$^{-3}$ $Zn^{2+}$. The $m$ values obtained are in the range mentioned in the literature [5]. The wide range of $m$ values found in the literature is due to various factors affecting the volume of gas evolving at the electrode surface. Therefore, when comparing results, such differences as the range of applied current density, the position, type, and the height of the electrode must be taken into account. The result of the present

*Table 2. Calculation of Sc, Sh, and ScRe numbers for different plating current densities in an electrolyte containing 50 g dm$^{-3}$ Zn, 100 g dm$^{-3}$ $H_2SO_4$, and 0.04 mg dm$^{-3}$ $Sb^{3+}$*

| c.d. (mA cm$^{-2}$) | 60 | 50 | 40 | 30 | 12 |
|---|---|---|---|---|---|
| $K_{Zn} \times 10^4$ (cm s$^{-1}$) | 5.7 | 5.4 | 4.9 | 4.2 | 3.8 |
| $I_{l,Zn}$ (mA cm$^{-2}$) | 89.21 | 84.7 | 76.8 | 66.5 | 59.6 |
| $\rho$ (g cm$^{-3}$) | 1.087 | 1.097 | 1.048 | 1.112 | 1.140 |
| $\nu \times 10^2$ (cm$^2$ s$^{-1}$) | 1.306 | 1.326 | 1.345 | 1.367 | 1.465 |
| *Sc* | 3436 | 3489 | 3540 | 3598 | 3856 |
| *Sh* | 224 | 212 | 193 | 167 | 149 |
| $\delta_{Zn} \times 10^3$ (cm) | 6.69 | 7.04 | 7.77 | 8.97 | 10.01 |
| *ScRe* | 597 | 498 | 398 | 298 | 239 |
| *ScGr* $\times 10^{-9}$ | 2.751 | 2.687 | 2.629 | 2.569 | 2.338 |

*Table 3. Calculation of Sc, Sh, and Sc · Re numbers for different plating current densities in an electrolyte containing 50 g dm$^{-3}$ Zn, 100 g dm$^{-3}$ $H_2SO_4$, and 0.08 mg dm$^{-3}$ $Sb^{3+}$*

| c.d. (mA cm$^{-2}$) | 60 | 50 | 40 | 30 | 12 |
|---|---|---|---|---|---|
| $K_{Zn} \times 10^4$ (cm s$^{-1}$) | 6.6 | 6.1 | 5.6 | 5.1 | 4.6 |
| $I_{l,Zn}$ (mA cm$^{-2}$) | 103.1 | 96.51 | 88.52 | 79.94 | 71.82 |
| $\rho$ (g cm$^{-3}$) | 1.098 | 1.105 | 1.112 | 1.121 | 1.144 |
| $\nu \times 10^2$ (cm$^2$ s$^{-1}$) | 1.328 | 1.436 | 1.367 | 1.394 | 1.481 |
| *Sc* | 3495 | 3542 | 3597 | 3667 | 3897 |
| *Sh* | 259 | 242 | 222 | 200 | 180 |
| $\delta_{Zn} \times 10^3$ (cm) | 5.79 | 6.18 | 6.47 | 7.47 | 8.31 |
| *ScRe* | 777 | 647 | 518 | 388 | 298 |
| *ScGr* $\times 10^{-9}$ | 2.680 | 2.627 | 2.570 | 2.501 | 2.306 |

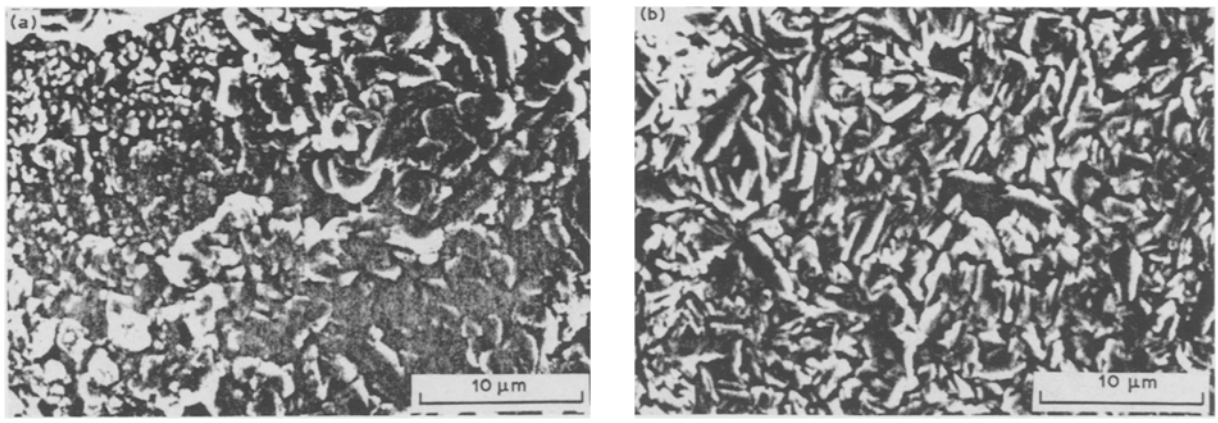


Fig. 6. Zn deposits obtained from an electrolyte containing 50 g dm$^{-3}$ Zn, 150 g dm$^{-3}$ $H_2SO_4$ at 0.08 mg dm$^{-3}$ $Sb^{3+}$ with (a) 20 mA cm$^{-2}$, (b) 80 mA cm$^{-2}$ current densities.

study also show the need to be aware of chemical effects such as antimony and acid concentrations.

### 3.3. *Empirical correlations*

Figure 10 shows that the mass transfer data for pure electrolytes are expressed by the following equation:

$$Sh = 12.47\,(ReSc)^{0.45} \quad (7)$$

The experimental data shown in Figure 11 for electrolytes containing antimony can be correlated as

$$Sh = 15.13\,(ReSc)^{0.42} \quad (8)$$

These equations provide satisfactory correlations for the present experimental work, wherein the correlations were envisaged in terms usually employed for forced convection. Accordingly, the values of these groups were calculated. Some of the physical properties used in the calculations were determined from experimental measurements of the electrolytes while others came from data available in the literature [20, 21].

The $Sh$ number = $KL/D$ was calculated using a 1.5 cm electrode length and measured $K_{Zn}$ and $D_{Zn}$ values. $Sc$ ($\nu/D$) was calculated using an average $\nu$ and $D_{Zn}$. The $Re$ number ($V_gL/\nu$) was calculated from current efficiency data and volume flux ($V_g/A$). The experimental value, $m = 0.45$, obtained in Equation 7 is close to the value of the exponents, 0.5, obtained for the penetration or microconvection models. The exponent, 0.33, of the hydrodynamic model is based mainly upon natural turbulent convection and no coalescence of bubbles. In general, the experimental results show that the increase in the order of magnitude of $K_{Zn}$ is below 2, therefore, the electrolyte flow conditions are not turbulent [11]. In addition, the bubbles generated at the electrode surface could be seen to coalesce and rise slowly. For these reasons the hydrodynamic model is not applicable for this experimental study.

The exponent, $m$, obtained experimentally, showed a tendency to decrease from 0.45 for a pure electrolyte to 0.42 for an electrolyte containing antimony. The decrease in the exponent is accompanied by an increase in the volume flux of gas. Therefore, the

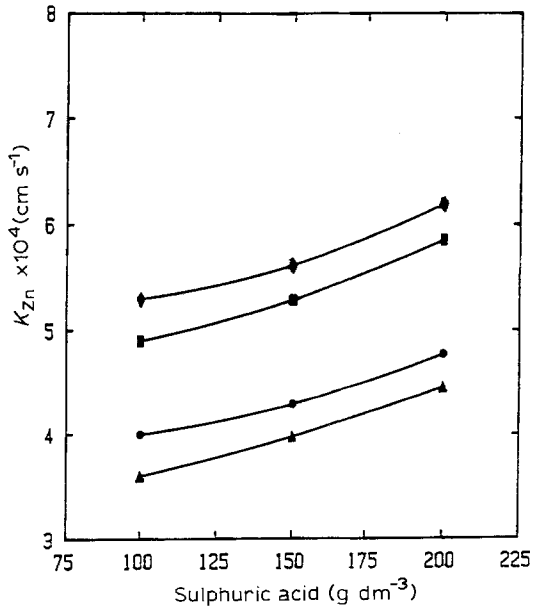


Fig. 7. Plot of $K_{Zn}$ values against $H_2SO_4$ concentrations at (▲ and ●) 30 mA cm$^{-2}$ and (■ and ◆) 60 mA cm$^{-2}$ for an alectrolyte containing 50 g dm$^{-3}$ Zn with 0.0 and 0.02 mg dm$^{-3}$ $Sb^{3+}$ concentrations.

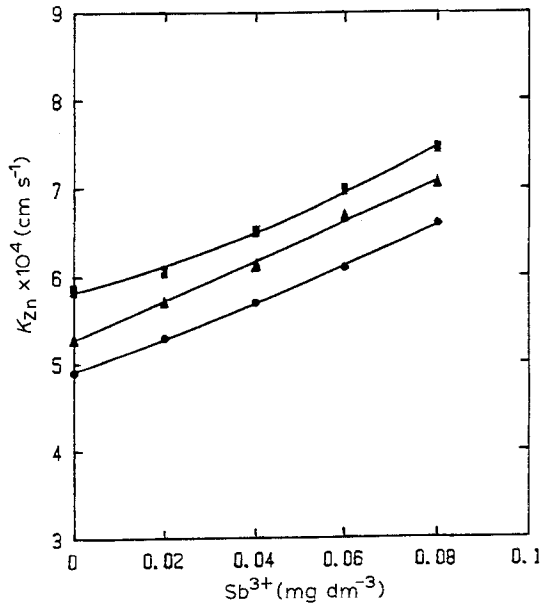


Fig. 8. The effect of $H_2SO_4$ and $Sb^{3+}$ concentrations on $K_{Zn}$ at 60 mA cm$^{-2}$. Sulphuric acid: (●) 100, (▲) 150 and (■) 200 g dm$^{-3}$.

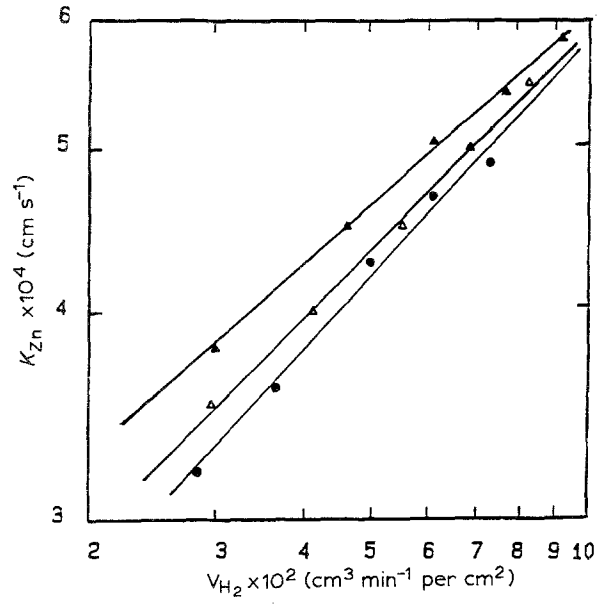


Fig. 9. The variation of $K_{Zn}$ with the volume flux of hydrogen gas at various $H_2SO_4$ concentrations: (●) 100, (△) 150 and (▲) 200 g dm$^{-3}$.

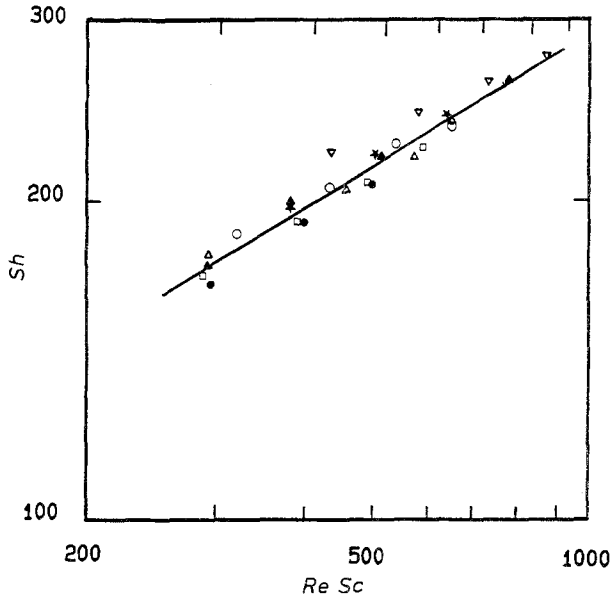


Fig. 11. Dimensionless representation of the mass transfer results for an acid electrolyte ($x$) with antimony additions ($y$), represented as ($x$ g dm$^{-3}$, $y$ mg dm$^{-3}$), respectively: (●) 100, 0.04; (*) 100, 0.08; (△) 150, 0.04; (▲) 150, 0.06; (○) 200, 0.02; (●) 200, 0.04 and (▽) 200, 0.06.

formation of eddies is increased and the coalescence of bubbles decreased. For this reason, it is plausible that an increase in the gas volume flux would decrease the exponent further. Under these circumstances, the hydrodynamic model might be expected to provide a good fit.

Attempts were made to represent the experimental results by Wilke's equation of the form $Sh = 0.66\ (GrSc)^{0.25}$, for natural convection only where the $Gr$ number $= gL^3(\rho_b - \rho_i)/\rho\nu^2$. The data did not correlate well. Furthermore, the $Sh$ numbers obtained were relatively independent of the $ScGr$ numbers, which indicated that the mass transfer was mainly enhanced by hydrogen evolution in addition to natural convection.

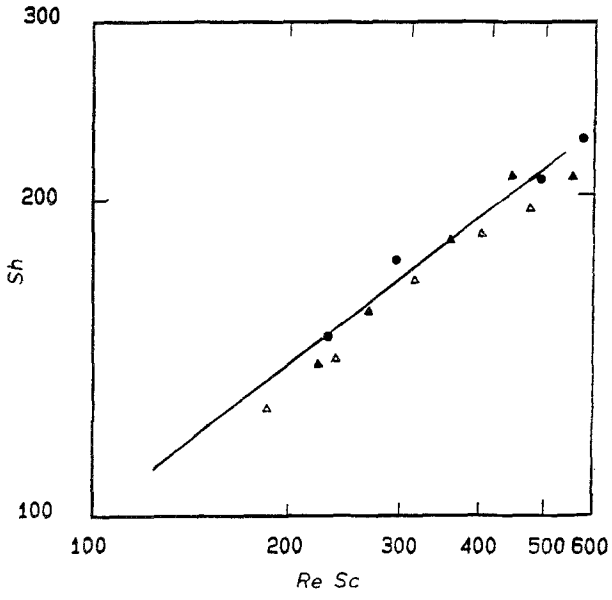


Fig. 10. Dimensionless representation of the mass transfer results for antimony-free electrolytes. Sulphuric acid concentration: (△) 100, (▲) 150 and (●) 200 g dm$^{-3}$.

## 4. Conclusions

The mass transfer coefficients of $Zn^{2+}$ in a non-sparged zinc sulphate electrolyte are increased significantly as the antimony additions increase. The presence of antimony in the electrolytes enhances the hydrogen evolution reaction and decreases the diffusion layer thickness. The line slope, $m$, of $K_{Zn}$ values versus the hydrogen volume flux is 0.44, which is in good agreement with literature values. The limiting current densities increase with increasing antimony additions. At a low current density such as 20 mA cm$^{-2}$, a significant change in deposition morphology is observed as the antimony additions increase. A noticeable dissolution of zinc deposits is obtained at higher levels of $Sb^{3+}$ such as 0.08 mg dm$^{-3}$ for an electrolyte containing 50 g dm$^{-3}$ $Zn^{2+}$, 150 g dm$^{-3}$ $H_2SO_4$. The results indicate that $K_{Zn}$ changes by a factor of 1.4 when the current density is increased from 12 to 60 mA cm$^{-2}$. The increase in $K_{Zn}$ in this case enhances the effect of the antimony such that it strongly influences the observed morphology (surface structure) of the deposit. In turn, the increase in $K_{Zn}$ is a consequence of the antimony increasing the volume flux of hydrogen. The results show the need to be aware of chemical effects, such as antimony and acid concentrations, in addition to conventional factors in mass transfer studies.

An empirical correlation in terms of the $Sh$, $Re$, and $Sc$ numbers has an exponent, $m$, of 0.45 for a synthetic electrolyte and 0.42 for an electrolyte containing antimony. The decrease in the exponent is accompanied by an increase in the volume flux of the hydrogen gas. The correlations agree with the exponent value of 0.5 associated with the penetration or microconvection models. The correlation provides a useful tool to

correlate the operating parameters in zinc electrowinning with mass transfer estimations.

## References


[1] L. J. J. Janssen, *Electrochim. Acta* **23** (1978) 81.
[2] M. G. Foud and G. H. Sedahmed, *ibid.* **18** (1973) 55.
[3] L. J. J. Janssen and J. G. Hoogland, *ibid.* **15** (1970) 1013.
[4] M. G. Foud, G. H. Sedahmed and H. A. El-Abd, *ibid.* **18** (1973) 279.
[5] H. Vogt, 'Comprehensive Treatise of Electrochemistry', Vol. 6, Plenum Press, New York (1983), Ch. 7, p. 457.
[6] P. J. Sides, *Tutorial Lectures in Electrochemical Eng. and Tech. II* **79** (1983) 226.
[7] N. Ibl and Venczel, *Metalloberflache* **24** (1970) 365.
[8] I. Rousar and V. Cezner, *Electrochim. Acta* **20** (1975) 289.
[9] K. Stephan and H. Vogt, *ibid.* **24** (1979) 11.
[10] L. J. J. Janssen and E. Barendrecht, *ibid.* **24** (1979) 693.
[11] F. Giron, G. Valentin, M. Lebouche and A. Strock, *J. Appl. Electrochem.* **15** (1985) 557.
[12] V. A. Ettel, B. V. Tilak and A. S. Gendron, *J. Electrochem. Soc.* **121** (1974) 867.
[13] T. J. O'Keefe, S. F. Chen, J. S. Cuzmar and V. A. Ettel, 'Application of Electrochemical Tracer Techniques for Determining Mass Transfer Conditions During Metal Deposition', Paper presented at 115th AIME Annual Meeting, New Orleans, LA, March 1986.
[14] S. F. Chen, Ph.D. Thesis, University of Missouri-Rolla (1986).
[15] A. Y. Hosny, T. J. O'Keefe and W. J. James, 'Minerals Engineering', Vol. 2, No. 3 Pergamon Press, Oxford (1989) pp. 415–423.
[16] P. Andrianne, J. S. Scoyer and R. Winand, *Hydrometallurgy* **6** (1980) 159.
[17] H. M. Wang, S. F. Chen, T. J. O'Keefe, M. Degrez and R. Winand, *J. Appl. Electrochem.* **19** (1989) 174.
[18] M. Degrez, A. Rodriguez Fajardo and R. Winand, *Oberfläche. Surface* **30** (9) (1989) 14.
[19] R. Winand, Electrocrystallization, in 'Application of Polarization Measurements in the Control of Metal Deposition' (edited by I. H. Warren) Amsterdam, The Netherlands, Elsevier Science Publishers B. V. (1984) pp. 47–83.
[20] E. W. Washburn, 'International Critical Tables', McGraw-Hill Book Co., New York (1929) p. 65.
[21] R. Parsons, 'Handbook of Electrochemical Constants', Butterworths Scientific, London (1959) p. 88.